Available online at www.sciencedirect.com

ScienceDirect

Nuclear Physics A 969 (2018) 94–113

NUCLEAR PHYSICS A

www.elsevier.com/locate/nuclphysa

Inclusive and exclusive measurements of alpha particle production mechanisms in the ^{7}Li + ^{144}Sm system

P.F.F. Carnelli [a,b,c,*], D. Martinez Heimann [a,b,c,**], A.J. Pacheco [a,b], A. Arazi [a,b], O.A. Capurro [a], J.O. Fernández Niello [a,b,c], M.A. Cardona [a,b], E. de Barbará [a], J.M. Figueira [a,b], D.L. Hojman [a,b], G.V. Martí [a], A.E. Negri [a,b,c]

[a] *Laboratorio TANDAR, Comisión Nacional de Energía Atómica, Av. Gral. Paz 1499, B1650KNA, San Martín, Buenos Aires, Argentina*

[b] *Consejo Nacional de Investigaciones Científicas y Técnicas, Godoy Cruz 2290, C1425FQB, CABA, Argentina*

[c] *Instituto de Investigación e Ingeniería Ambiental, Universidad Nacional de San Martín, 25 de Mayo y Francia, B1650BWA, San Martín, Buenos Aires, Argentina*

Received 4 July 2017; received in revised form 18 August 2017; accepted 28 August 2017
Available online 4 September 2017

Abstract

In this work we have studied the production of alpha particles emitted as a consequence of different reactions in the ^{7}Li + ^{144}Sm system at near-barrier energies. We have obtained absolute cross sections of the total yield at backward angles and at bombarding energies of 24 and 30 MeV. We have also performed complementary exclusive measurements of non-capture breakup processes at 30 MeV. In particular, the neutron transfer followed by non-capture breakup of the ^{6}Li ejectile, which was found to be the dominant process in the studied region, could be accounted for by estimations of a classical dynamical model. This contribution, together with estimations for the incomplete fusion and alpha particle evaporation following compound-nucleus formation, are compared to the experimental inclusive angular distributions obtained in this work.

* Principal corresponding author at: Instituto de Investigación e Ingeniería Ambiental, 25 de Mayo y Francia, B1650BWA, San Martín, Buenos Aires, Argentina.

** Corresponding author at: Instituto de Investigación e Ingeniería Ambiental, 25 de Mayo y Francia, B1650BWA, San Martín, Buenos Aires, Argentina.

E-mail addresses: pcarnelli@unsam.edu.ar (P.F.F. Carnelli), dheimann@unsam.edu.ar (D. Martinez Heimann).

http://dx.doi.org/10.1016/j.nuclphysa.2017.08.007
0375-9474/

Keywords: Low-energy heavy ion reactions; Alpha particle production; Weakly bound nuclei; Breakup reactions

1. Introduction

The reactions induced by weakly bound projectiles on heavy and medium-mass targets have been thoroughly studied over recent years (see Refs. [1–3] and references therein). The main interest lies in the possibility of understanding how different reaction mechanisms affect each other when the projectile presents a relatively small binding energy. Many of these weakly bound nuclei present cluster structures in their ground states that involve at least one alpha particle and, correspondingly, quite low energy thresholds for the breakup into α+X partitions. Therefore, it is relatively easy to excite this mode in any nuclear interaction, thus giving rise to a relatively large cross section for the production of alpha particles. In particular, breakup reactions are known to account in these cases for a significant part of the total reaction cross section and stable weakly bound nuclei are a useful alternative to investigate the various aspects of this kind of processes, also present in their radioactive counterparts. More so, it is matter of an ongoing debate regarding the connection between breakup and other reaction channels in the vicinity of the Coulomb barrier (CB). The relationship between breakup and fusion has been studied both experimentally [4–6] and theoretically [7–10] with focus on the much debated issue of whether breakup enhances or hinders the occurrence of fusion, and under which conditions one or the other effect might prevail.

It has also been observed that breakup can occur not only on the projectile itself but also on the ejectile produced after a transfer reaction. For example, for the ^{7}Li projectile (binding energy of 2.47 MeV), this mechanism could consist in either neutron stripping followed by the fragmentation of ^{6}Li into a deuteron and an alpha particle [11–14], or proton pickup followed by the breakup of ^{8}Be into two alpha particles [13]. Regardless of whether the nucleus that breaks up is the projectile or a projectile-like transfer product, the different processes can be classified according to the fate of the generated fragments: i) all the fragments are scattered away (non-capture breakup), ii) one of the fragments is captured by the target whereas the other scatters away (incomplete fusion), or iii) all breakup fragments are captured by the target (complete fusion following breakup) [15]. The experimental identification and characterization of those breakup reactions that evolve towards the subsequent capture of one or both fragments (also called capture breakup) usually presents more ambiguities. This happens because in general the fragments originated in these processes may be similar to, and may have similar energies than, the residues produced in complete fusion reactions.

In this work we present a study of the contributions of different mechanisms that produce alpha particles in reactions between the stable weakly bound ^{7}Li projectile and the spherical ^{144}Sm target at near-barrier energies ($E_{\mathrm{CB}} \simeq 24$ MeV) through inclusive and exclusive measurements. The inclusive method consisted in the measurement of angular distributions and energy spectra of emitted alpha particles. The exclusive measurements comprised the detection of alpha particles in coincidence with other light particles, mainly deuterons coming from the sequential transfer-breakup channel: $^{7}\mathrm{Li} + {}^{144}\mathrm{Sm} \rightarrow {}^{6}\mathrm{Li}^{*} + {}^{145}\mathrm{Sm} \rightarrow \alpha + \mathrm{d} + {}^{145}\mathrm{Sm}$ (see e.g. Ref. [12]). We analyze and discuss the energy spectra and angular distributions of the alpha particles by means of kinematic considerations related to the relevant mechanisms, the predictions of a statistical evaporation model for fusion processes [16] and also the predictions of a classical dynamical model for the description of breakup reactions [17].

The present study is part of our ongoing research plan that includes previous investigations on the ^{6,7}Li + ^{144}Sm systems. In particular, for the ^{6}Li + ^{144}Sm system we have also carried out studies of breakup effects through measurements of elastic [18] and inelastic scattering cross sections [19], of the alpha-particle production at extreme backward angles [20], and of the light particles emitted in coincidence as the result of non-capture breakup [21]. Works similar to the present one have also been done using other weakly bound stable (e.g. Refs. [22–28]) and radioactive (e.g. Refs. [29–34]) projectiles over a range of target masses, energies and angles.

In the following Section the experimental procedure is detailed. In Sect. 3 we describe the different data reduction processes applied. In Sect. 4 we analyze and discuss the results and, finally, in Sect. 5 we present the conclusions and outlook of this work.

2. Experimental procedure

The experimental work was carried out using the 20 UD tandem accelerator TANDAR of the National Atomic Energy Commission at Buenos Aires, Argentina. Beams of ^{7}Li with laboratory energies $E_{\rm lab} = 24$ and 30 MeV (typical intensities in the range of 1 to 15 pnA) were used to bombard a 96% enriched ^{144}Sm target, with a thickness of 60 μg/cm^2 (calculated from elastic scattering measurements). Since it is extremely difficult to get self-supported samarium targets of this thickness, a carbon backing of 20 μg/cm^2 nominal thickness was employed. The intensity of the ^{7}Li beam was determined by monitoring the elastically scattered particles on the ^{144}Sm target by means of a silicon surface barrier detector placed at 30° with respect to the beam direction, small enough to ensure pure Rutherford scattering for all the projectile energies.

For a subset of detector configurations, we performed independent measurements with a carbon target in order to evaluate the contribution of the backing in both the inclusive and exclusive experiments. For the inclusive measurements, it was found that this contribution was very important, hence a particular emphasis was placed in the procedure for its removal (see Sect. 3.1). On the other hand, the coincidence measurements were found to be almost unaffected by the backing since in this case the observed very low uniform background can be explained as stemming from random coincidences (see Sect. 3.2).

2.1. Inclusive measurements

The detection system used in the inclusive measurements was a position-sensitive telescope for particle identification that consists of a segmented-anode ionization chamber filled with P10 gas, followed by an array of three silicon position-sensitive detectors (PSDs). The angular acceptance of the whole device is 30°. We show a schematics of this detection system setup in Fig. 1(a). For each particle entering in the ionization chamber, the charge created by the energy loss along its path through the gas was collected by means of two successive anode segments. In this way, two partial energy loss signals ΔE_1 and ΔE_2 ($\Delta E = \Delta E_1 + \Delta E_2$) were produced. Finally, the particle was stopped in one of the three PSDs, which allowed the determination of the residual energy $E_{\rm res}$ and the position of incidence. The absolute energy calibration of the entire detection system was done using a triple alpha source (^{239}Pu–^{241}Am–^{244}Cm) and the elastically scattered ^{7}Li projectiles. The position calibration was carried out aligning a transit with two 1-mm-wide needles placed in front of each PSD.

The energy resolution of the whole system was determined in a separate experiment using different projectiles, bombarding energies and pressures of the ionization gas, and it was found to be

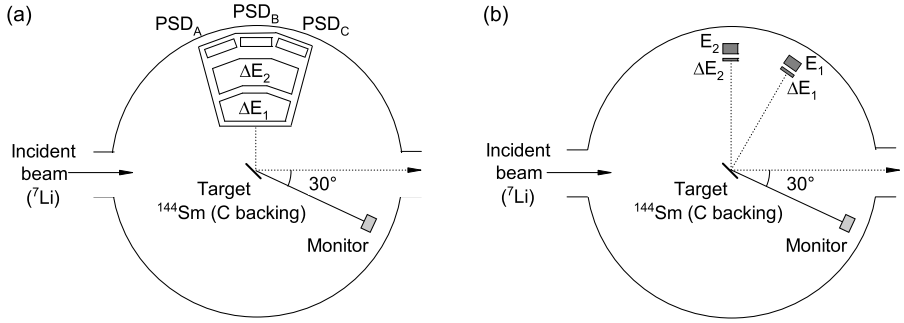

Fig. 1. Schematics of the experimental setups: (a) For the inclusive measurements we used a telescope composed by a ionization chamber and three position-sensitive detectors (PSDs) with a total angular acceptance $\Delta\theta = 30°$. (b) For the exclusive measurements the detection system consisted of two $E_{res} - \Delta E$ telescopes with an angular separation of approximately 17°. In both cases, a solid state detector was used at $\theta = 30°$ for normalization purposes. See text for details.

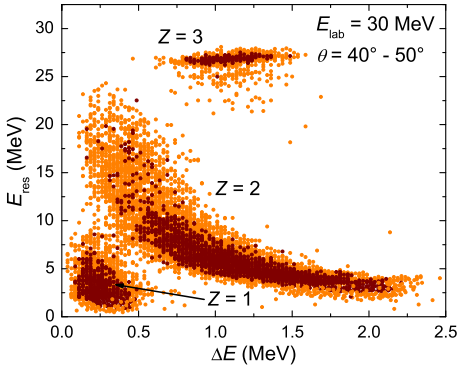

Fig. 2. (Color online) $E_{res} - \Delta E$ spectrum for the ^{7}Li + ^{144}Sm system at $E_{lab} = 30$ MeV obtained with the central PSD covering the $\theta = 40°-50°$ range, without any gates on the angular position.

better than 3% (FWHM/centroid). The angular uncertainty ranged from 0.2° to 0.3°, depending on the ionization gas pressure. For a more detailed description of this device see Ref. [35].

In these measurements, we used two projectile energies: $E_{lab} = 24$ and 30 MeV. Fig. 2 shows a bi-dimensional $E_{res} - \Delta E$ spectrum (without gates in angle) for the ^{7}Li + ^{144}Sm system at $E_{lab} = 30$ MeV. In this case the (position-integrated) E_{res} signals correspond to the central PSD covering the angular range $\theta = 40°-50°$ (in what follows, all angles will be expressed in the laboratory reference frame, unless noted differently). The effective solid angles subtended by the bins in which the PSDs were divided were obtained by elastic scattering measurements for the ^{16}O + ^{197}Au system at $E_{lab} = 50$ MeV. In order to complete an angular distribution, runs with the ionization chamber at four different angular positions were required: $\theta = 15°$–45°, 45°–75°, 75°–105°, and 105°–135°. For each position, an extra run was performed moving the detector by 5° in the backward direction to cover the dead zones between the PSDs. The irradiation time of each run was such that the number of events in the $Z = 2$ group (see Fig. 2) was around 3000 (2% statistical uncertainty). However, due to very small cross sections at backward angles, such requirement was relaxed to a few hundred events and/or the solid angles of the PSDs angular bins

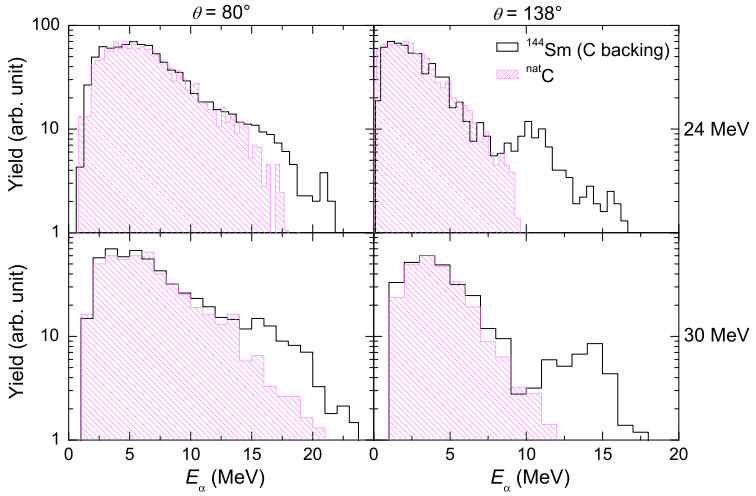

Fig. 3. (Color online) Inclusive energy spectra of the alpha particles emitted at $\theta = 80°$ and 138° for ^{7}Li projectiles at $E_{lab} = 24$ and 30 MeV impinging on a carbon-supported ^{144}Sm target and a carbon target. Each angle corresponds to the center of a $\Delta\theta = \pm 1.5°$ PSD bin.

were increased. These angular bins were defined during the data analysis dividing (by software) each PSD sensitive track.

A large number of inclusive alpha-particle energy spectra were obtained and analyzed, each one of them corresponding to different angular bins at different bombarding energies. Fig. 3 presents a couple of representative cases corresponding to 80° and 138° (backward range of our measurements) for both bombarding energies ($E_{lab} = 24$ and 30 MeV). In all cases, the angle θ corresponds to the center of a PSD bin for which an angular aperture $\Delta\theta = \pm 1.5°$ was defined by applying appropriate software cuts to the data. The histograms with empty areas represent the alpha-particle energy spectra obtained with the carbon-backed samarium target. To show the contribution stemming from the carbon backing, the equivalent spectra obtained with a pure carbon target (shaded areas) are also presented. For the purpose of a qualitative comparison, the spectra produced by the two targets shown in each panel of Fig. 3 have been arbitrarily normalized to their maximum values. From this very preliminary analysis we conclude that the contribution of the unwanted background might become increasingly important as the bombarding energy decreases and as the detection system moves to forward angles, as can also be expected from kinematic considerations.

2.2. *Exclusive measurements*

The non-capture breakup contribution was analyzed through coincident measurements performed at $E_{lab} = 30$ MeV. For this purpose two silicon $E_{res} - \Delta E$ telescopes mounted in the scattering chamber were used as is schematically shown in Fig. 1(b). The thicknesses were 1 mm for both E_{res} detectors and 30 (20) μm for ΔE_1 (ΔE_2). Typical angular acceptances of the detectors were $\Delta\theta \approx \pm 2°$. In general, the angular separation between telescopes was kept at the minimum possible value compatible with the geometry of the mountings, usually around 17°. At this fixed angular separation, the maximum angular range which could be covered by varying the position of both telescopes was $\theta = 45°$ to 135°. All the detectors were energy-calibrated using

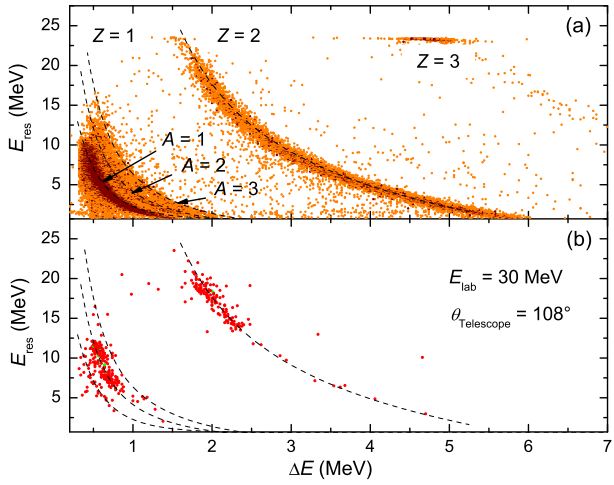

Fig. 4. (Color online) Two-dimensional E_{res} vs. ΔE spectra of the light particles emitted in the reaction ^{7}Li (30 MeV) + ^{144}Sm, detected in singles (a) and coincidence (b) modes by one of the telescopes, placed at $\theta = 108°$ (associated with a second telescope at $\theta = 92°$). The dashed curves are the calculated loci for ($Z = 1$, $A = 1, 2, 3$) and ($Z = 2$, $A = 4$).

a triple alpha source (^{239}Pu–^{241}Am–^{244}Cm) together with the measured ^{7}Li + ^{144}Sm elastic-scattering peak. The breakup products were detected using standard slow and fast coincidence techniques, either in singles or coincidence modes. The recorded parameters were the signals produced by the four solid-state detectors (ΔE_1, ΔE_2, E_{res1}, and E_{res2}) and the time-of-flight difference (ΔToF) between the fragments that hit each telescope. For that purpose we have used a time-to-amplitude converter (TAC) module whose fast start and stop input signals were provided by the preamplifiers associated to the ΔE detectors.

Fig. 4 shows typical two-dimensional E_{res} vs. ΔE spectra taken by one of the two telescopes in: (a) singles and (b) coincidence (any particle in each detector) modes. The dashed curves that are superimposed to the data points represent the calculated loci of various light particles for a wide range of energies. From Fig. 4(b) it can be seen that, while in singles mode protons seem to be the most abundant particles, coincident events involve mostly the detection of deuterons and alpha particles. These coincidence patterns will be discussed in detail in the following sections.

3. Data reduction

The whole body of data available from the reported experiments comprises: a) a total of 168 inclusive energy spectra of the alpha particles emitted in angular bins of average width $\Delta\theta = \pm 1.5°$ over the angular range 15° to 145°, and b) event-by-event files obtained from measurements in coincidence at the highest bombarding energy at six angular positions of the two-telescope system, covering the angular range from 50° to 130°.

3.1. Inclusive measurements

With the purpose of ensuring that all the alpha particles considered in each energy spectra were emitted only in reactions with ^{144}Sm nuclei, subtraction of the background coming from the carbon backing was necessary (see Fig. 3). Fig. 5 presents alpha particle spectra, both experimental and calculated, for three representative laboratory angles (80°, 115°, and 138°) at the

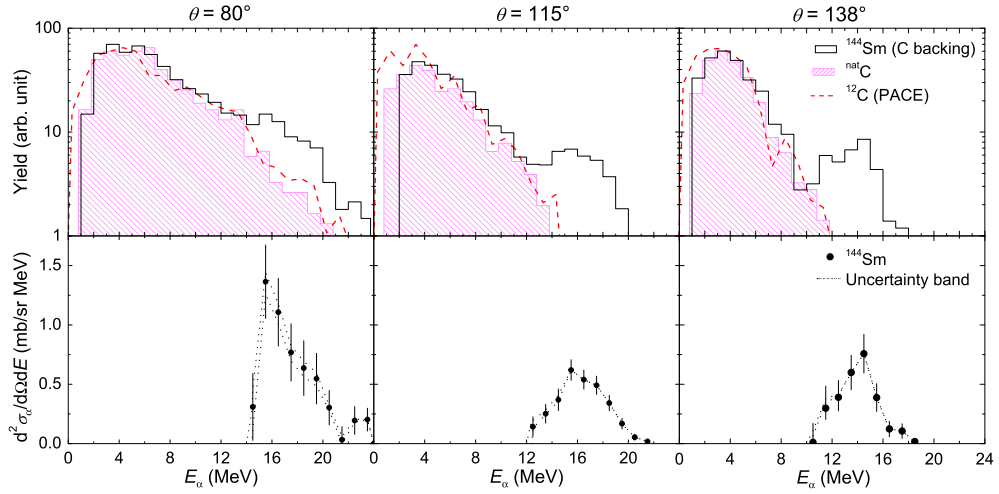

Fig. 5. (Color online) Upper row: Energy spectra at $E_{\rm lab} = 30$ MeV and $\theta = 80°$, 115°, and 138° from ^{7}Li projectiles on natural carbon (shaded area) and carbon-backed ^{144}Sm (empty area) targets compared with fusion-evaporation calculations from the ^{7}Li + ^{12}C system (PACE). Lower row: differential cross sections obtained by subtracting the fitted PACE calculations to the experimental samarium-target data (see text for details).

highest bombarding energy (30 MeV). Each panel of the upper row compares the experimental spectra obtained for natural carbon (shaded area) and carbon-backed ^{144}Sm (empty area) targets, under exactly the same geometrical configuration and the same conditions of the data analysis. In addition, the dashed curves show the energy distribution calculations of the alpha particles evaporated following compound nucleus reactions in the bombardment of ^{12}C with ^{7}Li projectiles, which were performed with the code PACE, version 2 [16]. For this calculations, we have chosen the fusion cross section estimated by the Bass model [36] with a l-diffuseness value of 0.3 $\hbar$ for the initial spin distribution (bombarding energies above the Coulomb barrier). The level density formalism of Gilbert and Cameron [37] was employed with a level density parameter of $a = A/7.5$ and the optical model parameters from PACE built-in systematics were chosen for the calculation of the transmission coefficients of particle emission. Concerning the remaining input parameters, we tested that the results of the statistical model calculations are quite insensitive to changes in them.

Given the excellent agreement between the results of PACE and the available data obtained with the carbon target, we decided to use similar calculations in order to subtract the contribution of the backing from the samarium target at all the measured angles. For that purpose, each one of the corresponding calculated spectra was normalized to fit the experimental spectrum (samarium plus carbon) within the energy region to which only the carbon backing is expected to contribute. The lower row of Fig. 5 shows, for these selected cases, the differential cross-sections obtained after subtracting the calculated carbon background from the samarium data. The uncertainty bands (dotted curves) of the differential cross-sections shown in the lower row of Fig. 5 were obtained from the fitting process by modifying the parameters so as to obtain a change in 1 unit of the χ^2/ν minimum value (being ν the degrees of freedom).

From the systematic application of this procedure it can be seen that at $E_{\rm lab} = 30$ MeV it is not possible to reliably separate the data of interest from the background for angles below $\theta \sim 60°$. In the case of $E_{\rm lab} = 24$ MeV, the angular limitation for a reliable separation of the alpha particles

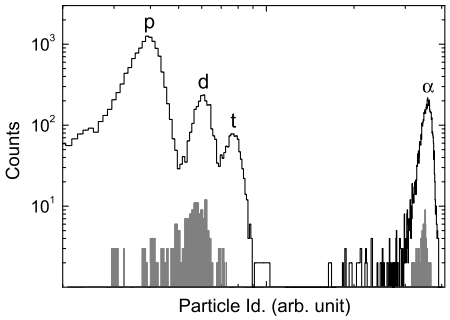

Fig. 6. Coincidence-gated spectrum (shaded area) superimposed over a singles-gated one (empty area) for the ^{7}Li + ^{144}Sm system ($E_{\rm lab} = 30$ MeV, $\theta_1 = 92°, \theta_2 = 108°$). Deuteron–alpha coincidences (d) resulted the dominant channel over proton–alpha (p), triton–alpha (t) and alpha–alpha (α).

coming from reactions with ^{144}Sm from those originated in the backing was found to be at approximately $\theta \geq 110°$.

3.2. Exclusive measurements

In what follows we describe the procedure applied for a full identification and characterization of the non-capture breakup events from the results of the coincidence measurements of light particles using the two-telescope detection setup. A more detailed discussion of the subject can be found in Ref. [21].

The most outstanding result from these measurements was the dominance of coincidence events between deuterons and alpha particles. This observation is confirmed by the spectra presented in Fig. 6, where we display the distribution of the particles detected by one of the two telescopes according to a parameter proportional to MZ^2 for particle identification, both for the case of singles (empty area) and coincidence (shaded area) modes. Each breakup mode was initially identified by means of appropriate gates set on the $E_{\rm res} - \Delta E$ spectra of both telescopes. True coincidences were subsequently selected from the analysis of the correlation between the time-of-flight difference (ΔToF) between the two particles and the residual energy recorded by either one of the telescopes. An example of such correlation and of the corresponding level of random coincidences is illustrated in Fig. 7(a) for the particular case of deuteron–alpha coincidences.

The group of events that resulted from this type of analysis for other breakup channel were further characterized through the study of the energy correlations between the coincident particles. As an example, Fig. 7(b) shows a two-dimensional spectrum of the residual energies recorded in both telescopes after selection of true coincidences for the deuteron–alpha breakup mode. For comparison, the data points are overlaid to different calculations done with the code SUPERKIN [38,39] that incorporate the actual detection geometry of the setup (distances from the target to each telescope, shape and dimensions of the entrance collimators) and the thicknesses of the ΔE detectors. For clarity of the presentation, the calculated positions of the individual events have been replaced by representative dashed curves that show just the average position predicted for the selected breakup channel (deuteron–alpha) and, as a reference, for other channels as well (deuteron–alpha, triton–alpha, alpha–alpha). In all the calculations we assume that the target is left in its ground state. The possible contribution of the carbon backing to the background, if we assume a representative breakup reaction for a carbon target, was evaluated through an additional

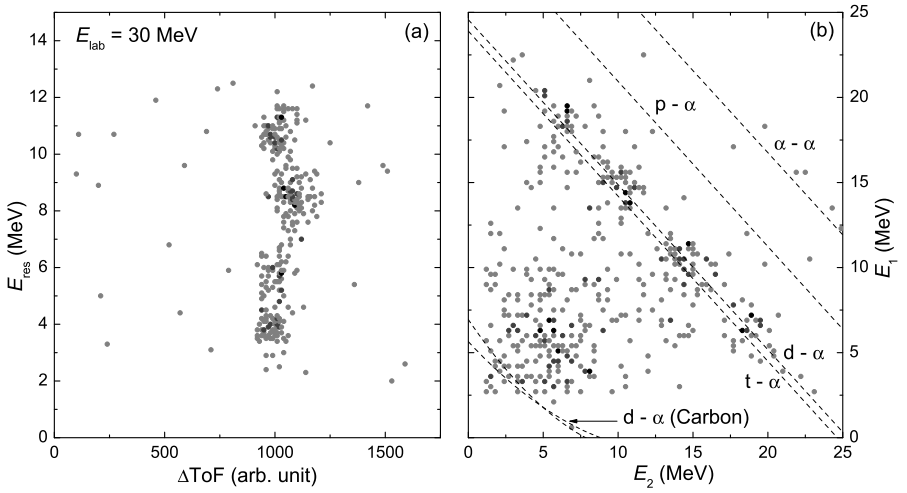

Fig. 7. a) Residual energy (E_{res}) vs. time-of-flight (ΔToF) difference spectrum for the deuteron–alpha channel used for the analysis and selection of true and random coincidences. b) Correlation between the residual energies (E_1 vs E_2) recorded in both telescopes for the deuteron–alpha channel after selection of true coincidences. The dashed curves correspond to the calculated positions for different breakup modes on a ^{144}Sm target. For the evaluation of the possible background introduced by the carbon backing, an additional calculation of one breakup mode is included for the case of a carbon target. All the calculations have been made with the code SUPERKIN assuming wide relative-energy distributions and both target and projectile in their ground states.

calculation. It can be seen that the corresponding results on the lower left corner of the spectrum are well separated from the region of interest for the samarium target.

The comparison between the data and the calculations in Fig. 7(b) shows that the bulk of the coincidence events that appear distributed in four groups are very well described by the curve for the corresponding deuteron–alpha breakup channel. The observed structure of the data is a known kinematic fingerprint of a narrow relative-energy distribution, thus it can be taken as an indication of a resonant decay. As shown in Fig. 8, this can be further studied by filtering and projecting the corresponding set of events onto the residual-energy axis of one of the telescopes and then by comparing the experimental results (shaded histogram) with the curves corresponding to calculations done under different assumptions. The solid curve corresponds to a calculation for a very narrow relative-energy distribution centered at a value of 0.712 MeV, which would in turn correspond to the excess kinetic energy expected after the decay of ^{6}Li from its first resonant 3^{+} state at an excitation energy of 2.18 MeV. The position of the calculated peaks describe very well the observed structure of the data and lend additional support to the interpretation that a ^{6}Li nucleus is actually formed during the reaction as the product of an intermediate neutron-transfer reaction prior to the occurrence of breakup. For comparison, the dotted curve shows the calculation for a different kinetic-energy distribution of the same breakup mode, an arbitrary uniform distribution from almost the threshold for the alpha–deuteron breakup of ^{6}Li (1.47 MeV) up to approximately the energy of the first resonance. Finally, the dashed curve illustrates the expected spectrum for the triton–alpha channel that would result from projectile breakup through the $7/2^{-}$ first resonant state of ^{7}Li at an excitation energy of 4.63 MeV. The three curves have been calculated assuming equal total yields over the respective ranges of relative energies. Therefore, even though the absolute normalization is arbitrary, the channels are comparable to each other and the amplitudes of the curves do reflect the actual geometric efficiency for each one of them.

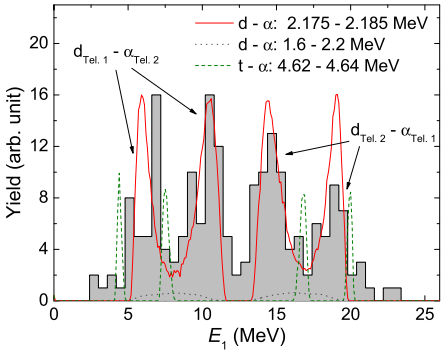

Fig. 8. (Color online) Projection of the correlated energy events from Fig. 7(b) onto the energy axis corresponding to telescope 1, together with numerical simulations for different relevant reaction channels. The absolute normalization is arbitrary, but the relative heights are directly related to the geometric detection efficiency. Deuteron–alpha coincidences turned out to be the most prominent breakup process measured.

Once classified, the analysis for the deuteron–alpha breakup mode involved the event-by-event transformation of the laboratory energies and scattering angles to a set of more physically meaningful variables [21], namely: a) the total reaction Q-value, b) the kinetic energy of the deuteron–alpha system in the ^{6}Li frame, $E_{\mathrm{d}-\alpha}$, c) the c.m. binary scattering emission angles θ_{Li} and ϕ_{Li}, and d) the breakup emission angles $\theta_{\mathrm{d}-\alpha}$ and $\phi_{\mathrm{d}-\alpha}$. Distributions of these relevant variables were produced taking advantage of the fact that the event-by-event handling of the raw data automatically takes care of the Jacobian of the transformation.

Finally, absolute breakup differential cross sections were obtained from the data. For this purpose we have applied a procedure extensively explained in Refs. [38,39], where the reader is suggested to refer for further details on the calculations. For the particular case of our experiments, the cross section that could be directly obtained from the data is $d^2\sigma/d\Omega_{\mathrm{d}-\alpha}d\Omega_{\mathrm{Li}}$ as a function of the binary scattering angles θ_{Li}, ϕ_{Li} and the breakup emission angles $\theta_{\mathrm{d}-\alpha}$, $\phi_{\mathrm{d}-\alpha}$. Lower-order differential cross sections can be obtained through integration over the whole range of the appropriate variables, although in most practical cases these sums should extend well beyond the regions that have reasonably high efficiencies. For our case, in order to calculate the partially integrated cross section $d\sigma/d\Omega_{\mathrm{Li}}$, we have incorporated the information contained in the binary and breakup angular distributions that we have measured in the present work, as a guide for the required interpolations and extrapolations. In this way, we obtained the differential cross section $d\sigma/d\Omega_{\mathrm{Li}}$ as a function of the binary angle θ_{Li} at 30 MeV bombarding energy.

With the appropriate adaptations, a very similar procedure to the one described above for the deuteron–alpha channel was also applied for the analysis of the triton–alpha and alpha–alpha breakup modes at 30 MeV. Due to the much lower geometric efficiencies, for these cases it was only possible to obtain upper bounds of the corresponding cross sections. The maximum values obtained in this way, expressed in units of the measured cross sections for the deuteron–alpha channel, were 0.77 for $\alpha - \mathrm{t}$ and 0.24 for α–α. As a reference it is useful to compare these upper bounds with the results obtained by Luong, et al. [13] for the same breakup channels, which were measured for the same reaction system but at a lower bombarding energy. By integration of the Q-value spectra presented in that work we can estimate the corresponding yields of the breakup channels under discussion in units of the α-d channel. For the case of $^7\mathrm{Li} \rightarrow \alpha + \mathrm{t}$ the value that we obtain from their data is 0.26 which is consistent with the results of our work. For the $^8\mathrm{Be} \rightarrow \alpha + \alpha$ channel the ratio obtained from Ref. [13] is 1.78, a value considerably larger

Table 1
Reactions that produce alpha particles in the ^{7}Li + ^{144}Sm system. Several other reactions, mostly with larger negative Q-values, are also possible but are not considered in this work. ER stands for "evaporation residue" and the asterisk indicates that the nucleus is in a highly excited state. Q-values are for ground states of the products in the final partitions, except for the one in parenthesis which corresponds to the respective intermediate partition, and the ones in brackets that correspond to the optimal values (for $E_{\mathrm{lab}} = 30$ MeV, see text for details).

Channel	Intermediate partition	Final partition	Q-value (MeV)
1 Complete fusion (CF)	^{151}Tb*	$\alpha + \mathrm{ER} + x\mathrm{n}$	(4.56)
2 Incomplete fusion (ICF)	$\alpha+^{147}$Eu*	$\alpha + \mathrm{ER} + x\mathrm{n}$	[−11.92]
3 t-transfer	$\alpha+^{147}$Eu*	$\alpha + \mathrm{ER} + x\mathrm{n}$	[−9.31]
4 Projectile non-capture breakup (^{7}Li-NCBU)		$\alpha + \mathrm{t} + ^{144}$Sm	−2.47
5 n-stripping → ejectile breakup (^{6}Li-NCBU)	^{6}Li+^{145}Sm	$\alpha + \mathrm{d} + ^{145}$Sm	−1.97
6 p-pickup → ejectile breakup	^{8}Be+^{143}Pm	$\alpha + \alpha + ^{143}$Pm	11.05
7 d-stripping → ejectile breakup	^{5}He+^{146}Eu	$\alpha + \mathrm{n} + ^{146}$Eu	−0.44
8 2n-stripping → ejectile breakup	^{5}Li+^{146}Sm	$\alpha + \mathrm{p} + ^{146}$Sm	4.22
9 p-stripping → ejectile ternary breakup	^{6}He+^{145}Eu	$\alpha + \mathrm{n} + \mathrm{n} + ^{145}$Eu	−7.63
10 Projectile ternary breakup		$\alpha + \mathrm{d} + \mathrm{n} + ^{144}$Sm	−8.72

than the upper bound obtained in the present work. Nonetheless the results of these comparisons should be evaluated cautiously since they correspond to different bombarding energies and, taking into account the particular geometry of each detection system, to different regions of the multidimensional space of relevant angular variables that describe the breakup process.

4. Results and discussion

A list of possible sources of alpha particles that could have important contributions to the present data and a summary of their basic characteristics is presented in Table 1. The second column of the table displays the products of a (real or virtual) intermediate stage useful solely for the purpose of characterization of each reaction. The third column lists the final products that would in principle be subject to actual detection, and the fourth column shows representative Q-values.

The complete-fusion reaction (channel 1) that occurs when the ^{7}Li projectile or all breakup fragments are captured by the ^{144}Sm target leads to an excited ^{151}Tb nucleus, which may subsequently decay through the emission of neutrons and, possibly, protons and/or alpha particles.

Incomplete fusion reactions leading to alpha-particle emission (ICF, channel 2) involve in turn the fusion of one of the breakup fragments with the target while the alpha particle flies away. The heavy reaction partner in this process (^{147}Eu, in our case) is left in a highly excited state resembling the formation of a compound nucleus that eventually decays via neutron evaporation and gamma ray emission of the successive residues. For this channel, the alpha-particle energy distributions have been obtained from the classical dynamical model described in Refs. [17,40] using the code PLATYPUS [41]. As an example, those calculated distributions for the case of 30 MeV bombarding energy and backward emission angles (135° to 140°) are approximately centered between 14 and 15 MeV, with FWHM values around 3 MeV (see Fig. 9). It is worth noticing that those predicted centroids are very close to the values that can be estimated under the simplified assumption that the emitted alpha particles from ICF reactions behave as unperturbed spectators whose asymptotic outgoing velocities are equal to those of the elastically scattered projectiles. At 30 MeV this condition is satisfied for an excitation energy of the ^{147}Eu nucleus

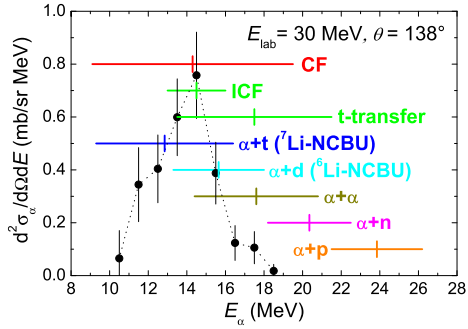

Fig. 9. (Color online) Inclusive energy spectrum of the alpha particles emitted in reactions with ^{7}Li projectiles at $E_{lab} =$ 30 MeV impinging on the carbon supported ^{144}Sm target for $\theta = 138.0° \pm 1.5°$. The labeled segments indicate the expected energy ranges of the alpha particles that would be emitted in reactions listed in Table 1. See text for details.

$E^* = 20.7$ MeV which corresponds to laboratory energies of the emitted alpha particles close to 14.5 MeV for the same angular range.

Direct triton-transfer reactions (channel 3) give rise to the same exit channel partition as that of ICF. Following the semi-classical approach proposed in Refs. [42,43] it is possible to estimate the optimal Q-value and the Q-window for t-transfer to occur. In our case these calculations lead to a distribution of alpha-particle energies centered at 17.5 MeV with a FWHM of 8.4 MeV (see Fig. 9).

Projectile non-capture breakup leading to the emission of a triton and an alpha particle (^{7}Li-NCBU, channel 4) is known to be one of the dominant processes at sub-barrier energies [13], with significant cross sections also at energies close and above the Coulomb barrier.

More complex processes that involve the non-capture breakup of a weakly bound nucleus are also important and can occur when the reaction is preceded or triggered by a transfer [13] (ejectile non-capture breakup). This may occur in different ways: n-stripping followed by the fragmentation of the formed ^{6}Li into an alpha particle and a deuteron (^{6}Li-NCBU, channel 5); proton pickup leading to the formation of the unbound ^{8}Be, which then breaks into two alpha particles (channel 6); deuteron stripping followed by the breakup of ^{5}He (channel 7); 2n-stripping and the consequent breakup of the ^{5}Li into an alpha particle and a proton (channel 8).

Alpha particles can also be produced in other channels leading to ternary breakup of the light transfer product mostly with large negative Q-values (e.g. channels 9 and 10).

The evolution of alpha-particle energy spectra, both in shape and intensity, as a function of the scattering angle contains substantial information on the emission sources. For the particular case of the various non-capture breakup modes listed in Table 1, even from simple kinematic considerations it is possible to quite accurately predict which of them could actually play a significant role in the description of the experimental energy distributions. This kind of analysis, using the code SUPERKIN, has been performed assuming uniform distributions of different widths of the center-of-mass energies of the breakup fragments (one of them being an alpha particle in all cases). The agreement (or lack thereof) between the calculated and experimental shapes and positions of the energy spectra allows us to make a preliminary classification of these breakup modes. Fig. 9 shows a schematic result of such kinematic analysis where the horizontal bars represent typical positions and widths of calculated alpha-particle energy distributions, compared to experimental data (CF, ICF and t-transfer calculations are also shown to present their energy relations and will be discussed later in this Section). According to Fig. 9 the resulting groups of

breakup modes, in decreasing order of plausibility for becoming candidates to explain the data, are the following:

(a) $^{7}\mathrm{Li} \rightarrow \alpha + \mathrm{t}$, $^{6}\mathrm{Li} \rightarrow \alpha + \mathrm{d}$,
(b) $^{8}\mathrm{Be} \rightarrow \alpha + \alpha$,
(c) $\alpha + \mathrm{n}$, $\alpha + \mathrm{p}$.

So far we have presented experimental data and calculations for $^{7}\mathrm{Li} + {}^{12}\mathrm{C}$ that show the position in energy of the carbon background (Fig. 5) and preliminary calculations showing the energy position of the alpha particles emitted in the $^{7}\mathrm{Li} + {}^{144}\mathrm{Sm}$ reaction (Fig. 9). All of this reinforces the validity of the proposed $^{12}\mathrm{C}$ background subtraction procedure and it will be made even more clear in what follows.

Taking into account the preliminary results from kinematic considerations, we have subsequently performed a more quantitative analysis of all the energy spectra, where reactions in group (c) have not been taken into account given their contribution is not significant. The partial contributions from different processes (complete fusion, incomplete fusion, direct triton transfer and non-capture breakup) to the total differential cross sections for alpha-particle production were calculated using the present exclusive data in combination with various theoretical models.

To estimate the cross section of the alpha-particle emission originated in $^{7}\mathrm{Li} + {}^{144}\mathrm{Sm}$ complete fusion reactions we have implemented the code PACE once again. For this, we made the same considerations as in Sect. 3.1 except that at near barrier energies (i.e., 24 MeV), we used the fusion partial cross sections calculated by the parameter-free double folding São Paulo potential (SPP) [44,45] as input of the statistical code.

The contributions from incomplete fusion and the non-capture breakup modes of group (a) have been calculated using the code PLATYPUS. For the case of $^{7}\mathrm{Li} \rightarrow \alpha + \mathrm{t}$ (projectile breakup) we used the values given by the systematics of Ref. [46] for the breakup parameters α and β. For the $^{6}\mathrm{Li} \rightarrow \alpha + \mathrm{d}$ mode, taking into account that the model can only consider the breakup of the projectile, we have followed the prescription of Ref. [47] by considering a $^{6}\mathrm{Li}$ pseudo-projectile (instead of the actual $^{7}\mathrm{Li}$ projectile) with values of the breakup parameters that were extracted from the exclusive measurements reported in Ref. [21]. In both cases, the corresponding nuclear potentials parameters were obtained from the systematics of Broglia and Winther [48,49].

Finite-range DWBA calculations for the direct triton transfer were carried out using the code FRESCO [50]. In this case we used the SPP for the real and imaginary parts of the $^{7}\mathrm{Li} + {}^{144}\mathrm{Sm}$ entrance channel potential (which successfully reproduces the elastic data of Ref. [18]). The same approach was used for the exit channel ($\alpha + {}^{147}\mathrm{Eu}$) and core-core ($\alpha + {}^{144}\mathrm{Sm}$) potentials. For the $\mathrm{t} + \alpha$ and $\mathrm{t} + {}^{144}\mathrm{Sm}$ binding potentials we used the optical parameters of Refs. [51] and [52], respectively.

Finally, we have been able to establish upper bounds for the cross sections of the $^{8}\mathrm{Be} \rightarrow \alpha + \alpha$ channel taking into account in detail the efficiency of our detection system for the coincidence measurements of this breakup mode (see Sect. 3.2). These maximum cross sections, that could be expressed as a fraction of the equivalent $^{6}\mathrm{Li} \rightarrow \alpha + \mathrm{d}$ yields, were subsequently used to normalize the shapes of the distributions calculated with the code SUPERKIN. As already mentioned, these calculations require in turn as an input the distribution of asymptotic kinetic energies of the alpha–alpha system; for this purpose we have chosen a uniform distribution in the range [0.5, 3.6] MeV, compatible with the experimental events observed for this reaction channel.

Fig. 10 shows an example of the comparison between the experimental absolute differential cross sections of the alpha-particle production and the calculations described above, for the par-

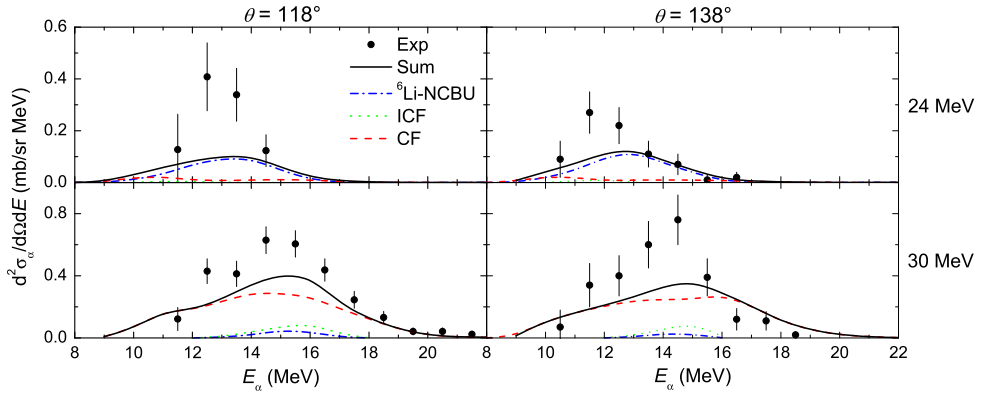

Fig. 10. (Color online) Quantitative analysis of alpha-particle energy spectra through the comparison of the inclusive experimental results with calculations for the predominant processes carried out with different models (see text for details). The upper panel corresponds to 24 MeV and the lower to 30 MeV bombarding energies, for each energy we show two laboratory angles: $\theta = 118°$ and 138°. The contributions of t-transfer, ^{7}Li-NCBU and $\alpha + \alpha$ processes are negligible.

ticular cases of two laboratory angles ($\theta = 118°$ and 138°) and at both bombarding energies (24 and 30 MeV). In addition to the individual contributions, Fig. 10 also shows as a solid curve the sum of them. In this calculation we excluded the $\alpha + p$ and $\alpha + n$ channels due to kinematic arguments. It can be seen in this figure that the contribution from the fusion-evaporation channel is dominant at 30 MeV whereas at 24 MeV it amounts to a small fraction (approximately 15%) of the total production of alpha particles. On the other hand, the non-capture $^{6}\mathrm{Li} \rightarrow \alpha + d$ channel, which is dominant at 24 MeV, does not contribute significantly at 30 MeV. Finally, alpha particles emitted from incomplete fusion reactions are predicted to make a small or moderate contribution at both bombarding energies. It ought to be noticed that all these calculated energy distributions overlap very reasonably with the experimental spectra. Although this is also true for direct triton transfer, and for the $^{7}\mathrm{Li} \rightarrow \alpha + t$ and $^{8}\mathrm{Be} \rightarrow \alpha + \alpha$ breakup modes, the cross sections are negligible and not visible when displayed using the vertical scale of Fig. 10. See the supplementary material for more example spectra corresponding to $E_{\mathrm{lab}} = 30$ MeV and at $\theta = 75°$ and 91°.

In Fig. 11 we summarize the experimental angular distributions of the total alpha-particle production cross section at both bombarding energies (full circles). For the purpose of comparison, the same angular range is displayed for both energies even though at 24 MeV only the alpha particles emitted at the most backward angles of this range could be discriminated. In the 30 MeV case, the experimental results for the ^{6}Li-NCBU measurement (empty circles) are also shown and were obtained assuming that the relative energies of the light breakup products in their center of mass system are negligible and therefore, that the laboratory velocities of those fragments are equal to the velocity of the ^{6}Li nucleus that breaks up. Additionally, this figure displays a prediction for the total cross section (solid curve) corresponding to the sum of complete fusion (dashed curve), incomplete fusion (dotted curve) and ^{6}Li-NCBU (dash-dotted curve) calculated contributions.

We can see that the experimental angular distribution of the total alpha-particle production obtained at 24 MeV does not show any important feature. On the other hand, at 30 MeV the most evident structure is a bump centered approximately at $\theta \simeq 78°$, which is related to the broad peak in the experimental angular distribution of the alpha-particle production obtained for the

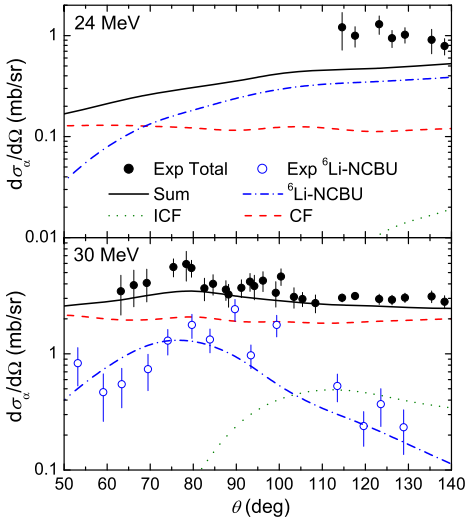

Fig. 11. (Color online) Laboratory angular distributions of alpha-particle production in the ^{7}Li + ^{144}Sm system at E_{lab} = 24 MeV (upper panel) and E_{lab} = 30 MeV (lower panel). We present experimental total (full circles) and ^{6}Li-NCBU (empty circles, only for 30 MeV) alpha-particle production cross sections. The experimental results of this work are compared with a prediction for the total cross sections (solid line) corresponding to the sum of three different calculated processes: CF (dashed curve), ICF (dotted curve) and ^{6}Li-NCBU (dash-dotted curve).

^{6}Li-NCBU process. At the energy above the barrier, the experimental ^{6}Li-NCBU cross section accounts for 27% of the total production cross section. Within the angular range where there are experimental data available for both bombarding energies, the integrated cross section of the total alpha-particle production at 30 MeV is approximately three times larger than at 24 MeV.

Comparing the experimental results with the calculations, at 24 MeV the main contribution comes from ^{6}Li-NCBU, representing 44% of the experimental production in the measured angular range. Complete fusion contributes in a 14% at this energy, while the incomplete fusion cross section is at least two orders of magnitude below the other two processes.

At 30 MeV the principal emission source within the measured angular range is complete fusion, which amounts to approximately 55% of the total experimental production. The angle-integrated contribution from the calculations of ^{6}Li-NCBU is approximately 20% of the total experimental production. This calculation is in very good agreement with the exclusive experimental data. Incomplete fusion is seen to contribute to the emission of alpha particles mostly at backward angles ($\theta \gtrsim 80°$) and the predicted integrated yield is less than 8% of the total experimental production.

The comparison between the ^{6}Li-NCBU 30 MeV data (empty circles) and the model calculation (dash-dotted curve) deserves some additional discussion. At the most forward angles the observed agreement owes to the fact that the breakup parameters used in the calculation have been extracted from those same data points, which happen to correspond to distant collisions for which non-capture breakup is expected to dominate over incomplete fusion. As we move to backward angles, corresponding to lower impact parameters, the model predicts an increasing contribution of the incomplete-fusion channel such that the calculated behavior of the remaining non-capture breakup component still agrees with the data. A question about the significance of the observed overall agreement arises in connection with the meaning of this incomplete-fusion (or capture breakup) component. In the present interpretation, this process would be presumably

associated to the breakup of a transfer product (^{6}Li in this case), rather than the breakup of the projectile itself. Although non-capture transfer-breakup is by now a well established mechanism, there is to date no direct experimental evidence for the existence of its capture counterpart.

In what respects only to calculations, at 24 MeV the ^{6}Li-NCBU contribution is approximately three times higher than the one corresponding to CF (for $114° \leq \theta \leq 138°$). In the same (limited) angular range, the contribution of ^{6}Li-NCBU (CF) is approximately five times higher (lower) than at 30 MeV. At this energy, the incomplete fusion cross section may seem negligible but in fact its contribution becomes a factor of two larger than that of ^{6}Li-NCBU at $\theta \gtrsim 105°$.

Finally, the solid curves shown in Fig. 11 for both energies are the sums of the sources considered in this analysis and should therefore be compared to the full-circle data points. For the relatively narrow angular range for which experimental data are available at 24 MeV, the sum of the theoretical predictions only describes 59% of the experimental results. On the other hand, at 30 MeV the calculations provide an acceptable description of the behavior exhibited by the data points and account for 83% of the integrated cross section.

5. Summary and conclusions

We have measured and analyzed the emission of alpha particles at backward angles in reactions induced by the bombardment of ^{144}Sm with the weakly bound ^{7}Li projectile at laboratory energies of 24 and 30 MeV. At the highest energy the inclusive data were complemented by the results obtained from the detection in coincidence of the emitted light particles in the same system.

From these experiments we have obtained absolute differential cross sections for the total alpha-particle emission and for the most intense transfer-breakup channel: $^7\text{Li} + {}^{144}\text{Sm} \rightarrow \alpha + \text{d} + {}^{145}\text{Sm}$. The predominance over other breakup processes is consistent not only with previous experimental results of different reaction systems and/or at different bombarding energies, but also it finds support in favorable Q-values and large relevant spectroscopic factors [53]. In addition, the inclusion of neutron-stripping followed by breakup in this reaction system has been shown to improve the theoretical description of quasi-elastic excitation functions at backward angles and the corresponding barrier distributions in this system [14].

For projectile breakup and for other transfer-breakup modes, in the best case, only upper limits of the cross sections could be obtained. In particular, for the $\alpha + \alpha + {}^{143}\text{Pm}$ channel, no similar theoretical support as in the case of transfer-breakup exists to our knowledge. The expectation of an important contribution from this process based on large positive Q-value (Table 1) and spectroscopic factor for proton-pickup [53] is not confirmed by the present experimental results.

The resulting distributions of alpha-particle energies at all measured angles have been analyzed in terms of the different possible contributions to the total yield. The component arising from complete fusion followed by particle evaporation was estimated using the standard statistical formalism. The contribution from different non-capture breakup channels and the plausibility of each one of them was preliminary evaluated by application of a kinematic analysis of the coincidences, that took into account in detail the geometry of the detection system. The strongest candidates emerging from such study were further investigated comparing the inclusive and exclusive data with the results of classical dynamical calculations. Apart from this, the direct triton transfer reaction was studied in the DWBA framework resulting in a negligible contribution at all the angles and energies considered in this work.

We have shown that the relative contributions from different sources to the total alpha-particle emission vary significantly when moving from the above-barrier towards the near-barrier regime.

Above the barrier, a fair and consistent agreement between the experimental and theoretical results is found. In particular, the agreement between the data and the calculation for the non-capture ^{6}Li$\rightarrow \alpha + d$ breakup mode, especially at the backward angles, raises questions about the existence of the associated capture (incomplete-fusion) mechanism, for which there is no direct experimental evidence. Within the limited angular range of the available data at the energy around the barrier (24 MeV), we observe that the calculations do not account for the total cross section. More data appears to be necessary at this near-barrier regime in order to confirm that other channel/s might be contributing to the alpha-particle production.

Acknowledgements

This work was supported by the Agencia Nacional de Promoción Científica y Tecnológica (ANPCyT, Argentina) [grant numbers PICT-2010-2018 and PICT-2013-1363] and the Consejo Nacional de Investigaciones Científicas y Técnicas (CONICET, Argentina).

Appendix A. Supplementary material

Supplementary material related to this article can be found online at https://doi.org/10.1016/j.nuclphysa.2017.08.007.

References

[1] L. Canto, P. Gomes, R. Donangelo, J. Lubian, M. Hussein, Recent developments in fusion and direct reactions with weakly bound nuclei, Phys. Rep. 596 (2015) 1–86, http://dx.doi.org/10.1016/j.physrep.2015.08.001.

[2] P.R.S. Gomes, J. Lubian, L.F. Canto, D.R. Otomar, D.R.M. Junior, P.N. de Faria, R. Linares, L. Sigaud, J. Rangel, J.L. Ferreira, E. Ferioli, B. Paes, E.N. Cardozo, M.R. Cortes, M.J. Ermamatov, P. Lotti, M.S. Hussein, Reactions with weakly bound nuclei, at near barrier energies, and the breakup and transfer influences on the fusion and elastic scattering, Few-Body Syst. 57 (3) (2016) 165–176, http://dx.doi.org/10.1007/s00601-015-1036-2.

[3] J.J. Kolata, V. Guimarães, E.F. Aguilera, Elastic scattering, fusion, and breakup of light exotic nuclei, Eur. Phys. J. A 52 (5) (2016) 123, http://dx.doi.org/10.1140/epja/i2016-16123-1.

[4] M. Dasgupta, P.R.S. Gomes, D.J. Hinde, S.B. Moraes, R.M. Anjos, A.C. Berriman, R.D. Butt, N. Carlin, J. Lubian, C.R. Morton, J.O. Newton, A. Szanto de Toledo, Effect of breakup on the fusion of ^{6}Li, ^{7}Li, and ^{9}Be with heavy nuclei, Phys. Rev. C 70 (2004) 024606, http://dx.doi.org/10.1103/PhysRevC.70.024606.

[5] J. Kolata, Transfer, breakup, and fusion reactions of ^{6}He with ^{209}Bi near the Coulomb barrier, Eur. Phys. J. A 13 (1–2) (2002) 117–121, http://dx.doi.org/10.1140/epja1339-22.

[6] C. Beck, F.A. Souza, N. Rowley, S.J. Sanders, N. Aissaoui, E.E. Alonso, P. Bednarczyk, N. Carlin, S. Courtin, A. Diaz-Torres, A. Dummer, F. Haas, A. Hachem, K. Hagino, F. Hoellinger, R.V.F. Janssens, N. Kintz, R. Liguori Neto, E. Martin, M.M. Moura, M.G. Munhoz, P. Papka, M. Rousseau, A. Sànchez i Zafra, O. Stézowski, A.A. Suaide, E.M. Szanto, A. Szanto de Toledo, S. Szilner, J. Takahashi, Near-barrier fusion of weakly bound ^{6}Li and ^{7}Li nuclei with ^{59}Co, Phys. Rev. C 67 (2003) 054602, http://dx.doi.org/10.1103/PhysRevC.67.054602.

[7] C.H. Dasso, R. Donangelo, Fusion enhancement via the soft dipole mode in neutron-rich nuclei, Phys. Lett. B 276 (1–2) (1992) 1–3, http://dx.doi.org/10.1016/0370-2693(92)90532-9.

[8] K. Hagino, A. Vitturi, C.H. Dasso, S.M. Lenzi, Role of breakup processes in fusion enhancement of drip-line nuclei at energies below the Coulomb barrier, Phys. Rev. C 61 (2000) 037602, http://dx.doi.org/10.1103/PhysRevC.61.037602.

[9] M.S. Hussein, M.P. Pato, L.F. Canto, R. Donangelo, Near-barrier fusion of ^{11}Li with heavy spherical and deformed targets, Phys. Rev. C 46 (1992) 377–379, http://dx.doi.org/10.1103/PhysRevC.46.377.

[10] K. Rusek, N. Alamanos, N. Keeley, V. Lapoux, A. Pakou, Breakup and fusion of ^{6}Li and ^{6}He with ^{208}Pb, Phys. Rev. C 70 (2004) 014603, http://dx.doi.org/10.1103/PhysRevC.70.014603.

[11] A. Shrivastava, A. Navin, N. Keeley, K. Mahata, K. Ramachandran, V. Nanal, V.V. Parkar, A. Chatterjee, S. Kailas, Evidence for transfer followed by breakup in ^{7}Li + ^{65}Cu, Phys. Lett. B 633 (4–5) (2006) 463–468, http://dx.doi.org/10.1016/j.physletb.2005.12.060.

[12] D.M. Heimann, A.J. Pacheco, A. Arazi, O.A. Capurro, P.F.F. Carnelli, D.S. Monteiro, J.O.F. Niello, J.M. Figueira, L. Fimiani, P. Grinberg, H.D. Marta, G.V. Martí, A.E. Negri, J.E. Testoni, Breakup reactions and exclusive measurements in the ^{6,7}Li + ^{144}Sm systems, AIP Conf. Proc. 1139 (1) (2009) 11–16, http://dx.doi.org/10.1063/1.3157791.
[13] D.H. Luong, M. Dasgupta, D.J. Hinde, R. du Rietz, R. Rafiei, C.J. Lin, M. Evers, A. Diaz-Torres, Predominance of transfer in triggering breakup in sub-barrier reactions of ^{6,7}Li with ^{144}Sm, ^{207,208}Pb, and ^{209}Bi, Phys. Rev. C 88 (2013) 034609, http://dx.doi.org/10.1103/PhysRevC.88.034609.
[14] D.R. Otomar, J. Lubian, P.R.S. Gomes, T. Correa, Breakup following neutron transfer for the ^{7}Li + ^{144}Sm system, J. Phys. G, Nucl. Part. Phys. 40 (12) (2013) 125105, http://dx.doi.org/10.1088/0954-3899/40/12/125105.
[15] P.R.S. Gomes, L.F. Canto, R. Donangelo, M.S. Hussein, Fusion and breakup of weakly bound nuclei, AIP Conf. Proc. 884 (1) (2007) 52–60, http://dx.doi.org/10.1063/1.2710557.
[16] A. Gavron, Statistical model calculations in heavy ion reactions, Phys. Rev. C 21 (1980) 230–236, http://dx.doi.org/10.1103/PhysRevC.21.230.
[17] A. Diaz-Torres, D.J. Hinde, J.A. Tostevin, M. Dasgupta, L.R. Gasques, Relating breakup and incomplete fusion of weakly bound nuclei through a classical trajectory model with stochastic breakup, Phys. Rev. Lett. 98 (2007) 152701, http://dx.doi.org/10.1103/PhysRevLett.98.152701.
[18] J.M. Figueira, J.O. Fernández Niello, A. Arazi, O.A. Capurro, P.F.F. Carnelli, L. Fimiani, G.V. Martí, D. Martinez Heimann, A.E. Negri, A.J. Pacheco, J. Lubian, D.S. Monteiro, P.R.S. Gomes, Energy dependence of the optical potential of weakly and tightly bound nuclei as projectiles on a medium-mass target, Phys. Rev. C 81 (2010) 024613, http://dx.doi.org/10.1103/PhysRevC.81.024613.
[19] A.E. Woodard, J.M. Figueira, D.R. Otomar, J.O. Fernández Niello, J. Lubian, A. Arazi, O.A. Capurro, P.F.F. Carnelli, L. Fimiani, G.V. Martí, D. Martinez Heimann, D.S. Monteiro, A.E. Negri, A.J. Pacheco, P.R.S. Gomes, Breakup coupling effects on near-barrier inelastic scattering of the weakly bound ^{6}Li projectile on a ^{144}Sm target, Nucl. Phys. A 873 (0) (2012) 17–27, http://dx.doi.org/10.1016/j.nuclphysa.2011.10.003.
[20] O.A. Capurro, A.J. Pacheco, A. Arazi, J.M. Figueira, D. Martinez Heimann, A.E. Negri, Breakup excitation function at backward angles from α-spectra in the ^{6}Li + ^{144}Sm system, Nucl. Phys. A 849 (1) (2011) 1–14, http://dx.doi.org/10.1016/j.nuclphysa.2010.10.001.
[21] D. Martinez Heimann, A.J. Pacheco, O.A. Capurro, A. Arazi, C. Balpardo, M.A. Cardona, P.F.F. Carnelli, E. de Barbará, J.O. Fernández Niello, J.M. Figueira, D. Hojman, G.V. Martí, A.E. Negri, D. Rodrígues, Differential and total cross sections of noncapture breakup reactions in the ^{6}Li + ^{144}Sm system, Phys. Rev. C 89 (2014) 014615, http://dx.doi.org/10.1103/PhysRevC.89.014615.
[22] G.R. Kelly, N.J. Davis, R.P. Ward, B.R. Fulton, G. Tungate, N. Keeley, K. Rusek, E.E. Bartosz, P.D. Cathers, D.D. Caussyn, T.L. Drummer, K.W. Kemper, α breakup of ^{6}Li and ^{7}Li near the Coulomb barrier, Phys. Rev. C 63 (2000) 024601, http://dx.doi.org/10.1103/PhysRevC.63.024601.
[23] D. Gupta, C. Samanta, A. Chatterjee, S. Kailas, B. Roy, K. Mahata, A. Shrivastava, Measurement of 42 MeV ^{7}Li projectile breakup on ^{208}Pb target near grazing incidence, Nucl. Phys. A 683 (1–4) (2001) 3–20, http://dx.doi.org/10.1016/S0375-9474(00)00452-8.
[24] C. Signorini, A. Edifizi, M. Mazzocco, M. Lunardon, D. Fabris, A. Vitturi, P. Scopel, F. Soramel, L. Stroe, G. Prete, E. Fioretto, M. Cinausero, M. Trotta, A. Brondi, R. Moro, G. La Rana, E. Vardaci, A. Ordine, G. Inglima, M. La Commara, D. Pierroutsakou, M. Romoli, M. Sandoli, A. Diaz-Torres, I.J. Thompson, Z.H. Liu, Exclusive breakup of ^{6}Li by ^{208}Pb at Coulomb barrier energies, Phys. Rev. C 67 (2003) 044607, http://dx.doi.org/10.1103/PhysRevC.67.044607.
[25] A. Pakou, N. Alamanos, A. Gillibert, M. Kokkoris, S. Kossionides, A. Lagoyannis, N.G. Nicolis, C. Papachristodoulou, D. Patiris, D. Pierroutsakou, E.C. Pollacco, K. Rusek, α-particle production in the reaction ^{6}Li+^{28}Si at near-barrier energies, Phys. Rev. Lett. 90 (2003) 202701, http://dx.doi.org/10.1103/PhysRevLett.90.202701.
[26] A. Pakou, N. Alamanos, N. Clarke, N. Davis, G. Doukelis, G. Kalyva, M. Kokkoris, A. Lagoyannis, T. Mertzimekis, A. Musumarra, N. Nicolis, C. Papachristodoulou, N. Patronis, G. Perdikakis, D. Pierroutsakou, D. Roubos, K. Rusek, S. Spyrou, C. Zarkadas, The ^{6}Li exclusive breakup on ^{28}Si at 13 MeV, Phys. Lett. B 633 (6) (2006) 691–695, http://dx.doi.org/10.1016/j.physletb.2005.11.088.
[27] F. Souza, C. Beck, N. Carlin, N. Keeley, R.L. Neto, M. de Moura, M. Munhoz, M.D. Santo, A. Suaide, E. Szanto, A.S. de Toledo, Reaction mechanisms in the ^{6}Li + ^{59}Co system, Nucl. Phys. A 821 (1–4) (2009) 36–50, http://dx.doi.org/10.1016/j.nuclphysa.2009.02.009.
[28] S.K. Pandit, A. Shrivastava, K. Mahata, N. Keeley, V.V. Parkar, P.C. Rout, K. Ramachandran, I. Martel, C.S. Palshetkar, A. Kumar, A. Chatterjee, S. Kailas, Probing transfer to unbound states of the ejectile with weakly bound ^{7}Li on ^{93}Nb, Phys. Rev. C 93 (2016) 061602, http://dx.doi.org/10.1103/PhysRevC.93.061602.
[29] J.J. Kolata, V.Z. Goldberg, L.O. Lamm, M.G. Marino, C.J. O'Keeffe, G. Rogachev, E.F. Aguilera, H. García-Martínez, E. Martinez-Quiroz, P. Rosales, F.D. Becchetti, T.W. O'Donnell, D.A. Roberts, J.A. Brown, P.A. DeY-

oung, J.D. Hinnefeld, S.A. Shaheen, Elastic scattering and transfer in the ^{8}Li+^{208}Pb system near the Coulomb barrier, Phys. Rev. C 65 (2002) 054616, http://dx.doi.org/10.1103/PhysRevC.65.054616.
[30] J.J. Kolata, H. Amro, F.D. Becchetti, J.A. Brown, P.A. DeYoung, M. Hencheck, J.D. Hinnefeld, G.F. Peaslee, A.L. Fritsch, C. Hall, U. Khadka, P.J. Mears, P. O'Rourke, D. Padilla, J. Rieth, T. Spencer, T. Williams, Breakup of ^{6}He incident on ^{209}Bi near the Coulomb barrier, Phys. Rev. C 75 (2007) 031302, http://dx.doi.org/10.1103/PhysRevC.75.031302.
[31] D. Escrig, A. Sánchez-Benítez, A. Moro, M. Álvarez, M. Andrés, C. Angulo, M. Borge, J. Cabrera, S. Cherubini, P. Demaret, J. Espino, P. Figuera, M. Freer, J. García-Ramos, J. Gómez-Camacho, M. Gulino, O. Kakuee, I. Martel, C. Metelko, F. Pérez-Bernal, J. Rahighi, K. Rusek, D. Smirnov, O. Tengblad, V. Ziman, α-particle production in the scattering of ^{6}He by ^{208}Pb at energies around the coulomb barrier, Nucl. Phys. A 792 (1) (2007) 2–17, http://dx.doi.org/10.1016/j.nuclphysa.2007.05.012.
[32] P.N. de Faria, R. Lichtenthäler, K.C.C. Pires, A.M. Moro, A. Lépine-Szily, V. Guimarães, D.R.J. Mendes, A. Arazi, A. Barioni, V. Morcelle, M.C. Morais, α-particle production in ^{6}He +^{120} Sn collisions, Phys. Rev. C 82 (2010) 034602, http://dx.doi.org/10.1103/PhysRevC.82.034602.
[33] V. Scuderi, A. Di Pietro, P. Figuera, M. Fisichella, F. Amorini, C. Angulo, G. Cardella, E. Casarejos, M. Lattuada, M. Milin, A. Musumarra, M. Papa, M.G. Pellegriti, R. Raabe, F. Rizzo, N. Skukan, D. Torresi, M. Zadro, Fusion and direct reactions for the system ^{6}He + ^{64}Zn at and below the Coulomb barrier, Phys. Rev. C 84 (2011) 064604, http://dx.doi.org/10.1103/PhysRevC.84.064604.
[34] M. Mazzocco, D. Torresi, D. Pierroutsakou, N. Keeley, L. Acosta, A. Boiano, C. Boiano, T. Glodariu, A. Guglielmetti, M. La Commara, J.A. Lay, I. Martel, C. Mazzocchi, P. Molini, C. Parascandolo, A. Pakou, V.V. Parkar, M. Romoli, K. Rusek, A.M. Sánchez-Benítez, M. Sandoli, O. Sgouros, C. Signorini, R. Silvestri, F. Soramel, V. Soukeras, E. Stiliaris, E. Strano, L. Stroe, K. Zerva, Direct and compound-nucleus reaction mechanisms in the ^{7}Be+^{58} Ni system at near-barrier energies, Phys. Rev. C 92 (2015) 024615, http://dx.doi.org/10.1103/PhysRevC.92.024615.
[35] P.F.F. Carnelli, A. Arazi, J.O. Fernández Niello, O.A. Capurro, M.A. Cardona, E. de Barbará, J.M. Figueira, D. Hojman, G.V. Martí, D. Martinez Heimann, A.E. Negri, A.J. Pacheco, A detection system with broad angular acceptance for particle identification and angular distribution measurements, Nucl. Instrum. Methods A 726 (0) (2013) 116–119, http://dx.doi.org/10.1016/j.nima.2013.05.182.
[36] R. Bass, Nucleus–nucleus potential deduced from experimental fusion cross sections, Phys. Rev. Lett. 39 (1977) 265–268, http://dx.doi.org/10.1103/PhysRevLett.39.265.
[37] A. Gilbert, A.G.W. Cameron, A composite nuclear-level density formula with shell corrections, Can. J. Phys. 43 (8) (1965) 1446–1496, http://dx.doi.org/10.1139/p65-139.
[38] D. Martinez Heimann, A.J. Pacheco, O.A. Capurro, Characterization of low-energy nuclear reactions involving emission of few non-relativistic particles, Nucl. Instrum. Methods A 622 (2010) 642–649, http://dx.doi.org/10.1016/j.nima.2010.07.063.
[39] D. Martinez Heimann, A.J. Pacheco, O.A. Capurro, Erratum to "Characterization of low-energy nuclear reactions involving emission of few non-relativistic particles", Nucl. Instrum. Methods A 622 (2010) 642–649, http://dx.doi.org/10.1016/j.nima.2012.08.054;
Nucl. Instrum. Methods A 694 (0) (2012) 313.
[40] A. Diaz-Torres, Modelling incomplete fusion dynamics of weakly bound nuclei at near-barrier energies, J. Phys. G 37 (7) (2010) 075109, http://dx.doi.org/10.1088/0954-3899/37/7/075109.
[41] A. Diaz-Torres, PLATYPUS: a code for reaction dynamics of weakly-bound nuclei at near-barrier energies within a classical dynamical model, Comput. Phys. Commun. 182 (4) (2011) 1100–1104, http://dx.doi.org/10.1016/j.cpc.2010.12.053.
[42] R. Broglia, G. Pollarolo, A. Winther, On the absorptive potential in heavy ion scattering, Nucl. Phys. A 361 (1) (1981) 307–325, http://dx.doi.org/10.1016/0375-9474(81)90480-2.
[43] W. von Oertzen, H.G. Bohlen, B. Gebauer, R. Künkel, F. Pühlhofer, D. Scühll, Quasi-elastic neutron transfer and pairing effects in the interaction of heavy nuclei, Z. Phys., a At. Nucl. 326 (4) (1987) 463–481, http://dx.doi.org/10.1007/BF01289551.
[44] L.C. Chamon, B.V. Carlson, L.R. Gasques, D. Pereira, C. De Conti, M.A.G. Alvarez, M.S. Hussein, M.A. Cândido Ribeiro, E.S. Rossi, C.P. Silva, Toward a global description of the nucleus–nucleus interaction, Phys. Rev. C 66 (2002) 014610, http://dx.doi.org/10.1103/PhysRevC.66.014610.
[45] M. Alvarez, L. Chamon, M. Hussein, D. Pereira, L. Gasques, E.R. Jr., C. Silva, A parameter-free optical potential for the heavy-ion elastic scattering process, Nucl. Phys. A 723 (1–2) (2003) 93–103, http://dx.doi.org/10.1016/S0375-9474(03)01158-8.
[46] O.A. Capurro, A.J. Pacheco, A. Arazi, P.F.F. Carnelli, J.O. Fernández Niello, D. Martinez Heimann, Systematics of the breakup probability function for ^{6}Li and ^{7}Li projectiles, Nucl. Phys. A 945 (2016) 186–196, http://dx.doi.org/10.1016/j.nuclphysa.2015.10.010.

[47] R. Rafiei, R. du Rietz, D.H. Luong, D.J. Hinde, M. Dasgupta, M. Evers, A. Diaz-Torres, Mechanisms and systematics of breakup in reactions of ^{9}Be at near-barrier energies, Phys. Rev. C 81 (2010) 024601, http://dx.doi.org/10.1103/PhysRevC.81.024601.

[48] W. Reisdorf, Heavy-ion reactions close to the Coulomb barrier, J. Phys. G 20 (9) (1994) 1297, http://dx.doi.org/10.1088/0954-3899/20/9/004.

[49] I. Dutt, R.K. Puri, Comparison of different proximity potentials for asymmetric colliding nuclei, Phys. Rev. C 81 (2010) 064609, http://dx.doi.org/10.1103/PhysRevC.81.064609.

[50] I.J. Thompson, Coupled reaction channels calculations in nuclear physics, Comput. Phys. Rep. 7 (4) (1988) 167–212, http://dx.doi.org/10.1016/0167-7977(88)90005-6, http://www.fresco.org.uk.

[51] F. Dunnill, T. Gray, H. Fortune, N. Fletcher, Optical parameters for the elastic scattering of ^{3}He by ^{4}He, Nucl. Phys. A 93 (1) (1967) 201–208, http://dx.doi.org/10.1016/0375-9474(67)90180-7.

[52] X. Li, C. Liang, C. Cai, Global triton optical model potential, Nucl. Phys. A 789 (1–4) (2007) 103–113, http://dx.doi.org/10.1016/j.nuclphysa.2007.03.004.

[53] S. Cohen, D. Kurath, Spectroscopic factors for the 1p shell, Nucl. Phys. A 101 (1) (1967) 1–16, http://dx.doi.org/10.1016/0375-9474(67)90285-0.